NANO LETTERS

Letter

pubs.acs.org/NanoLett

High Quality Factor Graphene-Based Two-Dimensional Heterostructure Mechanical Resonator

M. Will,[†] M. Hamer,[‡] M. Müller,[†] A. Noury,[§] P. Weber,[§] A. Bachtold,[§] R. V. Gorbachev,[‡] C. Stampfer,*[,†,∥] and J. Güttinger[†]

[†]JARA-FIT and 2nd Institute of Physics, RWTH Aachen University, 52074 Aachen, Germany

[‡]School of Physics and Astronomy and Manchester Centre for Mesoscience and Nanotechnology, University of Manchester, Oxford Road, Manchester M13 9PL, United Kingdom

[§]ICFO-Institut de Ciencies Fotoniques, The Barcelona Institute of Science and Technology, 08860 Castelldefels, Barcelona, Spain

[∥]Peter Grünberg Institute (PGI-9), Forschungszentrum Jülich, 52425 Jülich, Germany

Supporting Information

ABSTRACT: Ultralight mechanical resonators based on low-dimensional materials are well suited as exceptional transducers of minuscule forces or mass changes. However, the low dimensionality also provides a challenge to minimize resistive losses and heating. Here, we report on a novel approach that aims to combine different two-dimensional (2D) materials to tackle this challenge. We fabricated a heterostructure mechanical resonator consisting of few layers of niobium diselenide ($NbSe_2$) encapsulated by two graphene sheets. The hybrid membrane shows high quality factors up to 245,000 at low temperatures, comparable to the best few-layer graphene mechanical resonators. In contrast to few-layer graphene resonators, the device shows reduced electrical losses attributed to the lower resistivity of the $NbSe_2$ layer. The peculiar low-temperature dependence of the intrinsic quality factor points to dissipation over two-level systems which in turn relax over the electronic system. Our high sensitivity readout is enabled by coupling the membrane to a superconducting cavity which allows for the integration of the hybrid mechanical resonator as a sensitive and low loss transducer in future quantum circuits.

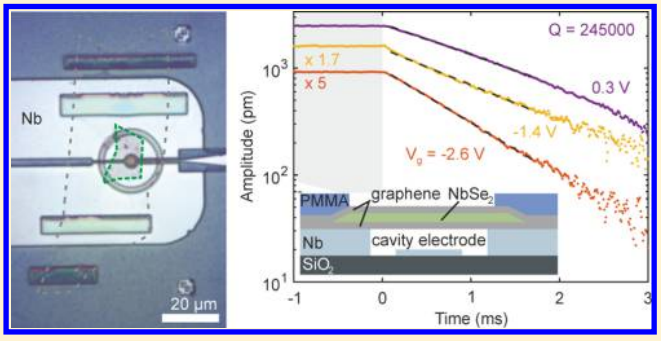

KEYWORDS: *Mechanical resonator, graphene, NbSe2, 2D heterostructures, NEMS, cavity readout*

The van der Waals heterostructures based on complementary two-dimensional (2D) materials are a topic of intense research[1,2] as they can be used to fabricate tailored electrical and optical devices with superior properties.[3−6] While mechanical devices based on individual 2D materials have shown tunable mechanical frequency and high quality factors,[7−14] the suitability of 2D heterostructures for mechanical resonators has not been explored so far. Another interesting question is how mechanical vibrations will interact with exotic states in encapsulated 2D materials such as 2D superconductors[6,15] or 2D magnets.[16,17]

In order to use heterostrucutres for mechanical applications, it is crucial that the mechanical quality factor is not significantly degraded by interlayer friction forces between the materials. So far, a detailed understanding of the energy dissipation in 2D mechanical resonators down to low temperatures is missing, despite various calculations[18−20] and experiments.[21−24] On the one hand, calculations on nanometer-sized few-layer graphene resonators suggest the importance of interlayer friction forces;[19] on the other hand, the highest quality (Q) factors were reported in multilayer graphene resonators.[11,14] Experimental limitations in studying the intrinsic mechanical dissipation are imposed by parasitic mechanical edge modes in doubly clamped devices,[22,24] mechanical spectral broadening due to amplitude and frequency noise[14,25] and the challenge of a noninvasive readout technique down to milikelvin temperatures.[14]

In this work, we demonstrate a high quality van der Waals heterostructure mechanical resonator based on few-layer niobium diselenide ($NbSe_2$) encapsulated by graphene. The membrane motion is sensitively probed by capacitive coupling to a superconducting microwave cavity. This readout technique is ideal to study the energy decay as it allows for time-resolved ring-down measurements which are independent of frequency fluctuations.[14,26] We demonstrate a high mechanical quality factor over 240,000 which compares favorably to the best multilayer graphene resonators.[7,9,11,14] Furthermore, by pulling the membrane electrostatically, the mechanical quality factor changes less compared with pure graphene resonators which can be explained by a reduced electrical resistance. By analyzing

Received: May 2, 2017
Revised: September 13, 2017
Published: September 14, 2017

DOI: 10.1021/acs.nanolett.7b01845
Nano Lett. 2017, 17, 5950−5955

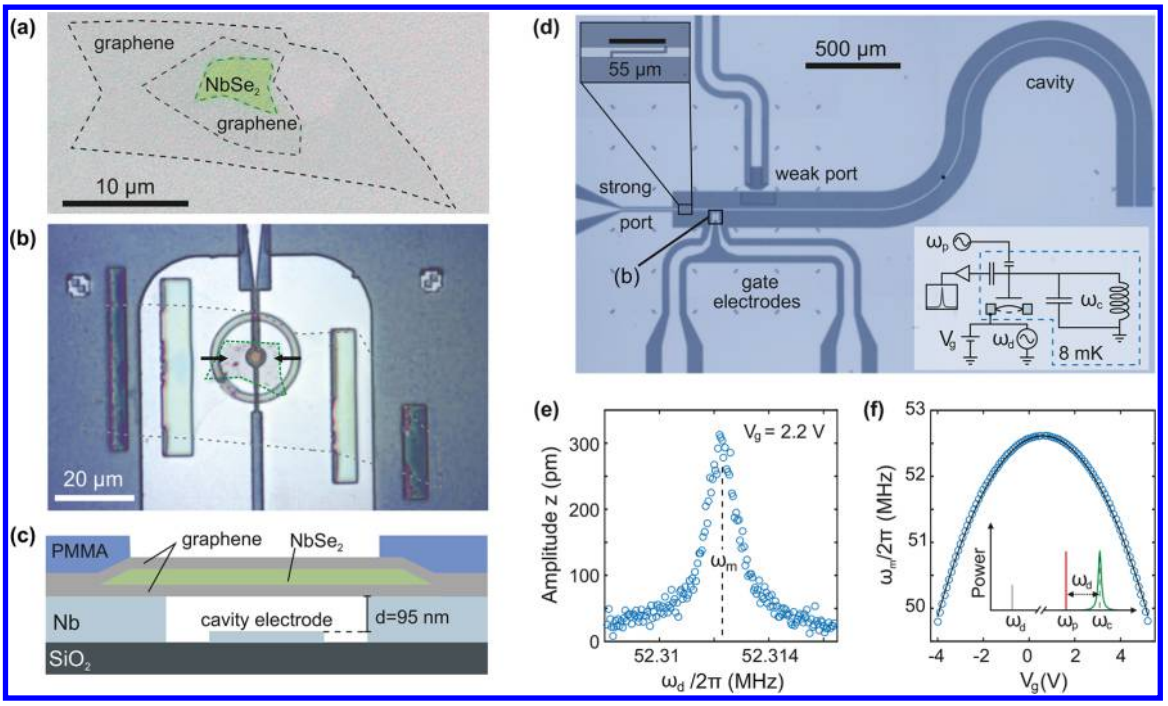

Figure 1. (a) Microscope image of the graphene/NbSe2/graphene assembly on the PMMA membrane before transfer to the microwave circuit. The single-layer nature of the graphene sheets is confirmed by Raman spectroscopy (see SI Section 2). The $NbSe_2$ flake consists of 3−4 layers according to optical contrast measurements. (b) Optical microscope image of the hybrid membrane after transfer onto the niobium (Nb) electrodes (light gray). The membrane is fixed to the electrodes by cross-linked PMMA stripes and a ring-shaped structure around the suspended device. (c) Schematic cross-section of the mechanical resonator along the black arrows in (b). The gate electrode allows to apply a potential between the membrane and the cavity electrode, displacing the membrane. The initial distance between the cavity electrode and the membrane is 95 nm. (d) Optical contrast image of the entire chip, showing the superconducting cavity including a weak and a strong coupling port and the two electrodes contacting the membrane. Inset: Schematic of the measurement setup. A microwave source with frequency ω_p is connected to the weak port and the cavity field is detected over the strong port at the cavity resonance frequency ω_c. A static membrane-cavity voltage V_g and an ac mechanical drive voltage at frequency ω_d is applied at the membrane. (e) Exemplary spectral measurement of the mechanical amplitude as a function of ω_d with the extracted mechanical resonance frequency ω_m. (f) Resonant frequency ω_m of the hybrid membrane as a function of V_g. For the measurement, we drive with a constant force $F_d = 4.46 \times 10^{-14}$ N (see SI Section 2). The inset shows that we pump the cavity with a red detuned pump tone such that $\omega_p = \omega_c - \omega_d$.

the low-temperature dependence of the intrinsic energy decay we find an anomalous temperature dependence in the highest Q resonators of both types. This finding can be well understood by modeling the dissipation with two-level fluctuators that mediate the dissipation of mechanical energy to the electronic bath.[27−29]

The optical image of the device in Figure 1 shows the graphene-$NbSe_2$ hybrid membrane, which is capacitively coupled to a superconducting niobium (Nb) cavity. The heterostructure is assembled in an argon atmosphere to avoid contamination and degradation of the $NbSe_2$ layer.[6] The membrane consists of few layers of $NbSe_2$ that are encapsulated by single-layer graphene flakes on each side (see Figure 1a). Alternatively, it is also possible to use hBN crystals or other stable 2D materials for the encapsulation. The main reason to use graphene is the high mechanical strength of the material and the minimal added effective mass by monolayer encapsulation. Another beneficial aspect of graphene is the ease to find single-layer graphene. We expect the $NbSe_2$ layer to induce superconductivity in the graphene due to the proximity effect. However, as the right contact showed an infinite resistance, we were not able to observe superconductivity in transport measurements. As previously demonstrated with few-layer graphene membranes,[9] the encapsulated membrane is transferred on top of a prepatterned Nb cavity and clamped by cross-linking the poly(methyl methacrylate) (PMMA) membrane that was used to transfer the 2D membrane (Figure 1b,c). The membrane is contacted over the left electrode which allows to apply a static gate voltage V_g and a resonant driving voltage V_d with respect to the grounded cavity electrode (Figure 1c,d). The as-fabricated device has an initial separation of d = 95 nm, which is weakly reduced by 8 nm for the maximum applied voltage of $V_g = -4$ V in this work. This static displacement is inferred from the shift of the cavity frequency $\omega_c/2\pi \approx 7.5$ GHz as a function of V_g due to the change of the cavity capacitance.[26] Tunable mechanical resonance frequencies, low mass, and high mechanical quality factors are key assets of mechanical resonators based on graphene. We show that these quantities can be maintained also in graphene-based heterostructure membranes. Figure 1e shows the spectral response of the hybrid resonator to a driving tone with a resonance frequency $\omega_m/2\pi > 50$ MHz. This frequency is comparable to drums with graphene membranes of similar radius to this $r = 1.7$ μm. The mechanical vibration is probed by the capacitive coupling between the electromagnetic pump field in the cavity and the mechanical motion.[9] The pump field is injected into the cavity over a weakly coupled port and the scattered field is detected over a strongly coupled port and amplified by a low noise amplifier at the 3.5 K stage of the cryostat (Figure 1d). For all measurements, we use a red-detuned pump tone such that the anti-Stokes scattered field becomes resonant with the cavity frequency (see inset Figure

DOI: 10.1021/acs.nanolett.7b01845
Nano Lett. 2017, 17, 5950−5955

1f). The coupling is characterized by the so-called single photon-phonon coupling constant $g_0/2\pi \approx 6.1$ Hz, which we estimate in SI Section 2. We use sufficiently low pump fields such that we can neglect optomechanical backaction. In order to evaluate the mass of the membrane we measure the V_g dependence of ω_m (see Figure 1f). The decrease of $\omega_m/2\pi$ with increasing $|V_g|$ is a hallmark of an electro-mechanical resonator under tension and can be attributed to a softening of the mechanical potential by the electric field. For the fundamental mode of a circular resonator, the gate voltage-dependent mechanical resonance frequency can be modeled by[9]

$$\omega_m(V_g) = \sqrt{\omega_0^2 - \frac{0.271\epsilon_0\pi r_g^2}{d^3 m_{eff}}(V_g - V_0)^2} \quad (1)$$

Here $\omega_0/2\pi$ is the maximum resonance frequency at the mechanical charge neutrality point (V_0 = 0.6 V), ϵ_0 is the electric constant, $m_{eff} = 0.27\pi r^2\rho_{2D}$ the effective mass of the fundamental mode, ρ_{2D} the two-dimensional mass density of the membrane and r_g = 1 μm the radius of the gate electrode. From a fit to the data, we obtain m_{eff} = 37.7 fg and $\omega_0/2\pi$ = 52.6 MHz. Given the radius of the membrane, this effective mass corresponds to the mass of roughly 20 layers of graphene with ρ_{gr} = 0.76 fg μm^{-2}. Considering that one layer of $NbSe_2$ (ρ_{NbSe2} = 4.1 fg μm^{-2}) has the mass of 5.2 graphene layers, the mass is in agreement with a heterostructure composed of three layers of $NbSe_2$ encapsulated by two layers of graphene and some extra mass that might be attributed to polymer residues from the fabrication. From ω_0, we can estimate the initial tension of the circular membrane[9]

$$\epsilon \approx \frac{\omega_0^2 m_{eff}}{4.92E_{2D}} = 0.08\% \quad (2)$$

with $E_{2D} = n_{gr}E_{2D,gr} + n_{NbSe_2}E_{2D,NbSe_2}$ the combined two-dimensional Young's modulus. Here $n_{gr(NbSe_2)}$ = 2 (3) is the number of graphene ($NbSe_2$) layers and $E_{2D,gr(NbSe_2)}$ = 340 Nm^{-1} (144 Nm^{-1}) is the elastic stiffness of graphene ($NbSe_2$).[30,31]

In order to probe the mechanical energy dissipation independent of frequency noise and mechanical nonlinearities, we perform ring-down measurements (see Figure 2). For this measurement, the mechanical resonator is driven to a constant amplitude until the drive is stopped at time t = 0 s and the decay of the amplitude is recorded as a function of time (Figure 2a). From the exponential energy decay $\propto e^{-\Gamma_{decay}t/2}$ the decay rate $\Gamma_{decay}/2\pi$ = 214 Hz is extracted at V_g = 0.3 V. The corresponding quality factor $Q = \omega_m/\Gamma_{decay}$ = 245,000 is among the highest measured so far in mechanical resonators based on 2D materials.[11,14]

Thanks to reduced electrical loss in our device, a high mechanical Q factor of $\approx 10^5$ is still maintained at increased gate voltage in contrast to few-layer graphene mechanical resonators.[11,26] In Figure 2b, the inverse mechanical quality factor obtained from energy decay measurements is plotted as a function of gate voltage V_g. The decrease of the quality factor can be attributed to electrical loss induced by capacitive displacement currents due to the motion of the membrane.[23,26] By increasing V_g, more charges have to flow to compensate the change of the capacitance induced by the mechanical motion. The resulting loss of mechanical energy can be described by

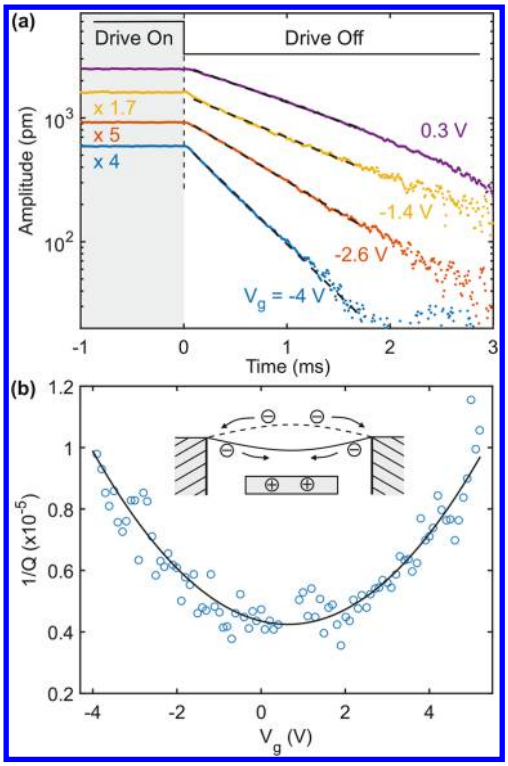

Figure 2. (a) Energy decay measurements at various V_g. The resonator drive is stopped at t = 0 s which leads to a subsequent decay of the mechanical amplitude. The plotted traces are the results of 10,000 averaged energy decay measurements. The highest quality factors are obtained at low gate voltage with values up to Q = 245,000 at V_g = 0.3 V. (b) V_g dependence of the inverse quality factor of the membrane (blue). Electronic dissipation is induced over capacitive displacement currents to compensate for the mechanical motion (schematic inset). The fitting parameter for the electronic dissipation is an effective resistance with R_{eff} = 50 Ω (black line, see text). Every point is the average of three measurements.

$$\frac{1}{Q_{Joule}} = \frac{R_{eff}}{m_{eff}\cdot\omega_m}\left(\frac{\partial C_m}{\partial z}\right)^2 (V_g - V_0)^2 \quad (3)$$

with R_{eff} an effective resistance of the membrane and $\partial C_m/\partial z$ the derivative of the capacitance with respect to the deflection z, which is obtained over the measured shift of the cavity resonance frequency as a function of V_g. The data agrees well with $1/Q = 1/Q_{Joule} + 1/Q_0$ with an intrinsic dissipation Q_0 = 237,000 and $R_{eff} \approx 50$ Ω (black line in Figure 2b). This effective resistance is comparable to the sheet resistance of a three layer $NbSe_2$ flake in the normal conducting state.[6]

Despite the apparent absence of superconductivity in the membrane the Joule dissipation is reduced by at least a factor of 4 in the heterostructure device compared with graphene-based mechanical resonators (see Table 1).

Table 1. Summary of Gate-Dependent Dissipation in Different Resonators (from References 14 and 26) in Comparison with Our Heterostructure Membrane Regarding Effective Resistance and Internal Quality Factor

membrane [layers]	R_{eff}	Q_0
30 × graphene	480 Ω	1.3 × 10^5
6 × graphene	220 Ω	10.6 × 10^5
2 × graphene, 3 × $NbSe_2$	50 Ω	2.37 × 10^5

DOI: 10.1021/acs.nanolett.7b01845
Nano Lett. 2017, 17, 5950−5955

By analyzing the temperature dependence of Q and ω_m in Figure 3, we find evidence that the quality factor is limited by

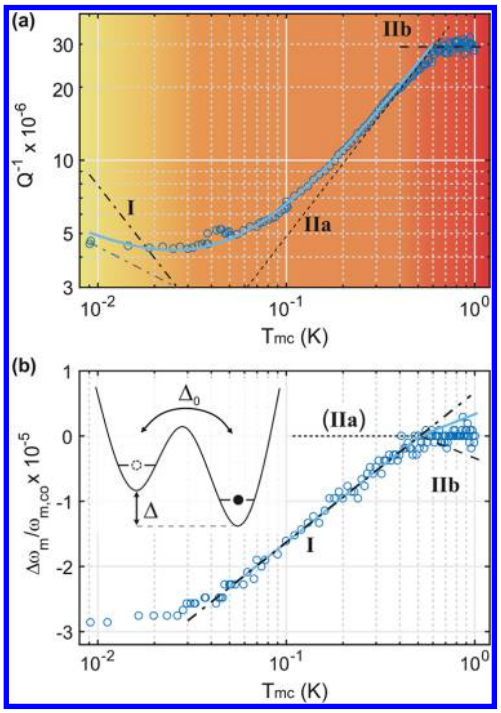

Figure 3. (a) Inverse quality factor Q^{-1} as a function of the cryostat temperature T_{mc}. The color shading highlights three different temperature regimes (yellow, orange, red). The temperature of the mixing chamber (mc) has been measured with a calibrated Magnicon noise thermometer. (b) Relative change of the resonance frequency $\Delta\omega_m/\omega_{m,co}$ as a function of cryostat temperature with respect to the resonance frequency $\omega_{m,co}/2\pi$ = 52.5745 MHz at T_{co} = 0.5 K. The inset depicts a sketch of a TLS with asymmetry Δ and tunneling coupling Δ_0. In panels (a) and (b), the different black lines correspond to the processes listed in Table 2. The blue line is the sum of the contributions from processes I and II. Note that in panel (a) the gray dot-dashed line with $Q^{-1} = 7 \times 10^{-7}\,(T_{mc}/\mathrm{K})^{-0.4}$ is used to fit the data in the yellow regime.

the coupling to two-level systems (TLS). Figure 3a shows the inverse quality factor as a function of cryostat temperature. The gate voltage was set to V_g = 0 V in order to minimize Joule heating losses and probe the intrinsic dissipation. Three different temperature dependencies are identified in the measurements indicated by the yellow, orange, and red shading in Figure 3a. We will focus first on the anomalous crossover at $T_{co} \approx 0.5$ K, which cannot be explained by adding two independent dissipation channels with $1/Q_1$ and $1/Q_2$ to $1/Q_{tot} = 1/Q_1 + 1/Q_2$. This is because the stronger temperature dependence would dominate at higher temperatures. It is important to note that this behavior is not related to the heterostructure type of our membrane as a very similar dependence has been observed in a $Q \approx 10^6$ few-layer graphene resonator (see SI Section 3). Looking at previous low-temperature measurements in graphene or nanotube-based resonators[24,32−34] a proportionality of Q^{-1} to T or $T^{1/3}$ has been observed individually. However, an increase of the temperature dependence at lower temperature has not been reported before. We attribute this difference to the higher precision and reduced heating involved in the detection with a superconducting cavity combined with ring-down measurements. Next we will show that these features can be understood in the framework of two-level fluctuators that are relaxed by the interaction with conduction electrons.

We now recall the model of a two-level fluctuator or tunneling system, which has been proposed to describe low-temperature effects in a wide range of isolating and metallic glasses and crystalline resonators.[27,28,34−43] In its simplest form, the tunneling system is defined by an energy asymmetry Δ and a matrix element Δ_0[28] for tunneling between the two states (see inset in Figure 3b). For the description of the physics, it is often helpful to characterize two-level systems over its energy splitting $E = (\Delta^2 + \Delta_0^2)^{1/2}$ and relaxation rate τ^{-1}. Because the resonator interacts with an ensemble of two-level systems, a specific distribution for both E and τ^{-1} is assumed depending on the exact modeling.[41] The mechanical motion interacts with the TLS over a periodic modulation of the potential. Thereby the TLS can absorb mechanical energy that is subsequently emitted in the phonon or electron bath providing a mechanical energy decay channel. The absorption process of the TLS can be either resonant (I) or over relaxation absorption (II).

(I) Resonant absorption is dominant at low temperatures where $k_B T \approx E \approx \hbar\omega_m$. The standard TLS model predicts $Q^{-1} \propto \tanh(\hbar\omega_m/(2k_B T))$ and a resonance frequency shift $\Delta\omega_m/\omega_{m,co} \propto \ln T$ for this process.[28] The effects of resonant absorption can be saturated once the mechanical pumping rate gets stronger than the relaxation rate.

(II) Absorption relaxation is dominant for $k_B T \approx E \gg \hbar\omega_m$. In this process, the mechanical strain fluctuations are affecting the TLS energy mainly over changes in the asymmetry energy Δ.[28] The resulting modulation of E influences the interaction of the TLS with thermal phonons and electrons. This process gives rise to the peculiar kink in the temperature dependence at T_{co} = 0.5 K, where the fastest relaxation rate τ_{min}^{-1} equals the mechanical frequency at T_{co}. In the following, we will discuss this process for both temperatures smaller (IIa) and larger (IIb) than T_{co}. (IIa) For $T < T_{co}$ where $\tau_{min}^{-1} \ll \omega_m$ there is a strong temperature dependence of the dissipation with $Q^{-1} \propto T^3$ for phonon relaxation and a linear dependence $Q^{-1} \propto T$ for relaxation over conduction electrons.[27] Electronic relaxation leads to a greatly reduced relaxation time which lowers T_{co} from a few Kelvin to the sub Kelvin regime for megahertz resonators.[28] The associated contribution to the frequency shift is negligible, so that the T dependence of ω_m is given by resonant absorption processes involving TLS with $E \approx \hbar\omega_m$, leading to $\Delta\omega_m/\omega_{m,co} \propto \ln(T)$. (IIb) At $T > T_{co}$ where $\tau^{-1}{}_{min} \gg \omega_m$ the relaxation is faster than the mechanical modulation and the dissipation rate is proportional to ω_m. The resulting damping is $Q^{-1} \approx \pi\, C/2$. The resonance frequency shift due to IIb is negative with $\Delta\omega_m/\omega_{m,co} = -1/2\, C \ln(T/T_0)$. The combined effect of I and II predicts a reduced but still positive frequency dependence. The positive dependence is not visible in the measurement and might be counteracted by a negative temperature dependence, for example, due to the negative thermal expansion of graphene (see SI Figure S5). Note that above a few Kelvin the temperature dependence is expected to become negative due to the onset of absorption relaxation by phonons.[28]

A quantitative comparison between theory and experiment is generally difficult and will serve here only to get a qualitative understanding of the parameters. We compare our measurements with the standard TLS theory.[28,41] We assume that electronic relaxation dominates over phonon relaxation in the measured temperature regime due to the low T_{co} (fast relaxation time) and $Q^{-1} \propto T$ below T_{co}. From the frequency

DOI: 10.1021/acs.nanolett.7b01845
Nano Lett. 2017, 17, 5950−5955

dependence we extract $T_{co} \approx 0.5$ K from the kink position and $C_\omega = 1 \times 10^{-5}$ from the slope below T_{co} (see formulas in Table 2). Note that the frequency offset has been adjusted such that

Table 2. Predictions for $\Delta\omega_m/\omega_{m,co}$ and Q^{-1} Based on the Standard TLS Theory in Metallic Systems[28a]

quantity	process	standard TLS model	
$\frac{\Delta\omega_m}{\omega_{m,co}}$	I	$C \ln\left(\frac{T}{T_0}\right)$	$\rightarrow C_\omega = 1 \times 10^{-5}$
	IIa	≈ 0	
	IIb	$-\frac{1}{2} C \ln\left(\frac{T}{T_{co}}\right)$	$\rightarrow T_{co} \approx 0.5$ K
Q^{-1}	I	$\pi C \tanh\left[\frac{\hbar\omega_m}{2k_BT}\right]$	(saturable)
	IIa	$\frac{\pi^3 C}{24} K^2 \frac{k_BT}{\hbar\omega_m}$	$\rightarrow K = 0.071$
	IIb	$\frac{\pi}{2} C$	$\rightarrow C_Q = 1.9 \times 10^{-5}$

[a]For both quantities, the contribution from resonant (I) and relaxation absorption (II) add up. The crossover temperature T_{co} separates the different contribution of relaxation absorption for $T \ll T_{co}$ (IIa) and for $T \gg T_{co}$ (IIb). T_0 depends on the frequency offset where $\Delta\omega_m = 0$ and is related to the crossing temperature T_{co}. The parameter C is related to the TLS density and the coupling strength of deformations to the TLS energy splitting. The parameter K is proportional to the conduction electron density and their coupling to TLS.

the temperature T_0 corresponding to $\Delta\omega_m = 0$ equals T_{co}. From the saturation of Q^{-1} for $T > T_{co}$, we extract $C_Q = 1.9 \times 10^{-5}$. The difference between C_ω and C_Q might arise from changes in the density of the contributing TLS at the different temperatures.[40] We extract a TLS electron coupling constant of $K = 0.071$ (dotted line) from the fit of the linear temperature dependence of contribution IIa. The temperature dependence in a high Q graphene device yields comparable values with $C_\omega = 1.6 \times 10^{-5}$ and $K = 0.089$ (see SI Section 3). These values are also in the same range that has been measured previously in metallic glasses and polycrystalline metals with $C = 10^{-5}$–10^{-4} and $K = 0.02$–0.2.[41,44] At the lowest temperatures, the dissipation has a negative temperature dependence as predicted by theory (see also SI Figure S3). However, the measurement shows a reduced temperature dependence compared to the model (I), which might be explained by insufficient thermalization of the membrane to the mixing chamber plate at the lowest temperatures ($T_{mc} < 40$ mK, see Figure 3b). Please note that the fit merely emphasizes the change of sign in temperature dependence and is not meant to be universally valid. In the low temperature Q^{-1} dependence of the graphene device, we do not observe any signature from process I. This might be explained with a complete saturation of the resonant TLS at the lowest drive amplitudes studied. Furthermore, in contrast to ref 45 we do not observe a saturation of the damping with increasing drive power but rather an increase in damping attributed to additional decay channels.[14] A deviation from the theoretical prediction of the standard model is not unexpected as it has been observed before in metallic glasses.[27] A nonsaturable attenuation might arise from more asymmetric TLS or a modified scattering cross-section.[44] Additionally, the effect of individual TLS with E and τ^{-1} deviating from the assumed contribution is enhanced due to the tiny volume of the membrane.[46]

The microscopic mechanism of TLS damping in 2D membranes is unclear so far. A previous calculation on dissipation in graphene and carbon nanotube resonators investigated electrically active TLS in the surrounding of the vibrating structure and concluded that the resulting dissipation will be negligible.[18] However, residues from fabrication or imperfections in the crystal might still contain mechanically activated TLS.[34]

TLS damping is not a universal limitation in 2D material-based mechanical resonators. In resonators with lower Q factors, we observe usually a saturation or reduced temperature dependence at low temperatures. This might be related to clamping induced loss[18] or loss over parasitic modes[22,24] which masks the effect of the TLS.

We have not found any indication for superconductivity in the measured heterostructure device. First, the electric resistance extracted from the dissipation as a function of gate voltage is compatible with normal conducting $NbSe_2$. Second, we would expect the superconductivity to suppress the coupling of the TLS to electrons below $T_c/2$,[28,42] which would lead to a higher kink temperature and increased temperature dependence compared to the measured data.

In conclusion, we presented a mechanical resonator based on van der Waals heterostructures of two-dimensional materials. The high mechanical quality, frequency tunability, and low electrical resistivity measured in a graphene/$NbSe_2$/graphene resonator exemplifies the opportunities of 2D heterostructures for mechanical resonators. The enhanced and partially linear temperature dependence of the dissipation is understood with mechanically mediated relaxation of two-level systems by conduction electrons. It might be possible to further improve the mechanical quality by using electrically isolating boron nitride for the encapsulation or reducing polymer residues in the fabrication. In future experiments, the combination of superconductivity and low mass in a 2D membrane opens the potential for ultralow loss and high sensitivity mechanical resonators. This is because a superconducting mechanical resonator suppresses electrical losses induced by mechanical motion and allows for higher pumping fields in a cavity based readout. Both are important for the exploration of quantum motion and improvements of force sensitivity in atomically thin mechanical resonators.[9–11,26]

■ ASSOCIATED CONTENT

Supporting Information

The Supporting Information is available free of charge on the ACS Publications website at DOI: 10.1021/acs.nanolett.7b01845.

Membrane characterization by Raman, calculation of resonator amplitude, data on temperature-dependent dissipation in additional devices, effect of thermal expansion on resonance frequency, and dependence of dissipation on mechanical drive voltage (PDF)

■ AUTHOR INFORMATION

Corresponding Author

*E-mail: stampfer@physik.rwth-aachen.de.

ORCID

M. Müller: 0000-0002-1852-6372

A. Bachtold: 0000-0002-6145-2479

Notes

The authors declare no competing financial interest.

DOI: 10.1021/acs.nanolett.7b01845
Nano Lett. 2017, 17, 5950–5955

■ ACKNOWLEDGMENTS

We thank Uwe Wichmann for help on the electronics and for fruitful discussions. Support by the Helmholtz Nano Facility (HNF)[47] at the Forschungszentrum Jülich, the Excellence Initiative (RWTH Start-Up Grant), the ERC-carbonNEMS and the ERC-GQEMS (GA-Nr. 280140) are gratefully acknowledged. The work is further supported by the ERC Advanced Grant 692876, the Foundation Cellex, Severo Ochoa (SEV-2015-0522), the Grant FIS2015-69831-P of MINECO, and the Fondo Europeo de Desarrollo Regional (FEDER).

■ REFERENCES

(1) Novoselov, K. S.; Mishchenko, A.; Carvalho, A.; Castro Neto, A. H. *Science* **2016**, *353*, aac9439.
(2) Liu, Y.; Weiss, N. O.; Duan, X.; Cheng, H.-C.; Huang, Y.; Duan, X. *Nat. Rev. Mats.* **2016**, *1*, 16042.
(3) Dean, C.; Young, A.; Meric, I.; Lee, C.; Wang, L.; Sorgenfrei, S.; Watanabe, K.; Taniguchi, T.; Kim, P.; Shepard, K.; J, H. *Nat. Nanotechnol.* **2010**, *5*, 722−726.
(4) Britnell, L.; Ribeiro, R. M.; Eckmann, A.; Jalil, R.; Belle, B. D.; Mishchenko, A.; Kim, Y.-J.; Gorbachev, R. V.; Georgiou, T.; Morozov, S. V.; Grigorenko, A. N.; Geim, A. K.; Casiraghi, C.; Neto, A. H. C.; Novoselov, K. S. *Science* **2013**, *340*, 1311−1314.
(5) Koppens, F.; Mueller, T.; Avouris, P.; Ferrari, A.; Vitiello, M.; Polini, M. *Nat. Nanotechnol.* **2014**, *9*, 780−793.
(6) Cao, Y.; et al. *Nano Lett.* **2015**, *15*, 4914−4921.
(7) Eichler, A.; Moser, J.; Chaste, J.; Zdrojek, M.; Wilson-Rae, I.; Bachtold, A. *Nat. Nanotechnol.* **2011**, *6*, 339−342.
(8) Lee, J.; Wang, Z.; He, K.; Shan, J.; Feng, P. X.-L. *ACS Nano* **2013**, *7*, 6086−6091.
(9) Weber, P.; Güttinger, J.; Tsioutsios, I.; Chang, D. E.; Bachtold, A. *Nano Lett.* **2014**, *14*, 2854−2860.
(10) Song, X.; Oksanen, M.; Li, J.; Hakonen, P. J.; Sillanpää, M. A. *Phys. Rev. Lett.* **2014**, *113*, 027404.
(11) Singh, V.; Bosman, S. J.; Schneider, B. H.; Blanter, Y. M.; Castellanos-Gomez, A.; Steele, G. A. *Nat. Nanotechnol.* **2014**, *9*, 820.
(12) Castellanos-Gomez, A.; Singh, V.; van der Zant, H. S. J.; Steele, G. A. *Ann. Phys.* **2015**, *527*, 27−44.
(13) Morell, N.; Reserbat-Plantey, A.; Tsioutsios, I.; Schädler, K. G.; Dubin, F.; Koppens, F. H. L.; Bachtold, A. *Nano Lett.* **2016**, *16*, 5102−5108.
(14) Güttinger, J.; Noury, A.; Weber, P.; Eriksson, A. M.; Lagoin, C.; Moser, J.; Eichler, C.; Wallraff, A.; Isacsson, A.; Bachtold, A. *Nat. Nanotechnol.* **2017**, *12*, 631−636.
(15) Xi, X.; Zhao, L.; Wang, Z.; Berger, H.; Forro, L.; Shan, J.; Mak, K. F. *Nat. Nanotechnol.* **2015**, *10*, 765−769.
(16) Lee, J.-U.; Lee, S.; Ryoo, J. H.; Kang, S.; Kim, T. Y.; Kim, P.; Park, C.-H.; Park, J.-G.; Cheong, H. *Nano Lett.* **2016**, *16*, 7433−7438.
(17) Chittari, B. L.; Park, Y.; Lee, D.; Han, M.; MacDonald, A. H.; Hwang, E.; Jung, J. *Phys. Rev. B: Condens. Matter Mater. Phys.* **2016**, *94*, 184428.
(18) Seoánez, C.; Guinea, F.; Castro Neto, A. H. *Phys. Rev. B: Condens. Matter Mater. Phys.* **2007**, *76*, 125427.
(19) Kim, S. Y.; Park, H. S. *Appl. Phys. Lett.* **2009**, *94*, 101918.
(20) von Oppen, F.; Guinea, F.; Mariani, E. *Phys. Rev. B: Condens. Matter Mater. Phys.* **2009**, *80*, 075420.
(21) Chen, C.; Rosenblatt, S.; Bolotin, K.; Kalb, W.; Kim, P.; Kymissis, I.; Stormer, H.; Heinz, T.; Hone, J. *Nat. Nanotechnol.* **2009**, *4*, 861−867.
(22) Zande, A. M. v. d.; Barton, R. A.; Alden, J. S.; Ruiz-Vargas, C. S.; Whitney, W. S.; Pham, P. H. Q.; Park, J.; Parpia, J. M.; Craighead, H. G.; McEuen, P. L. *Nano Lett.* **2010**, *10*, 4869−4873.
(23) Song, X.; Oksanen, M.; Sillanpää, M. A.; Craighead, H. G.; Parpia, J. M.; Hakonen, P. J. *Nano Lett.* **2012**, *12*, 198−202.
(24) Takamura, M.; Okamoto, H.; Furukawa, K.; Yamaguchi, H.; Hibino, H. *Micromachines* **2016**, *7*, 158.
(25) Miao, T.; Yeom, S.; Wang, P.; Standley, B.; Bockrath, M. *Nano Lett.* **2014**, *14*, 2982−2987.
(26) Weber, P.; Güttinger, J.; Noury, A.; Vergara-Cruz, J.; Bachtold, A. *Nat. Commun.* **2016**, *7*, 12496.
(27) Golding, B.; Graebner, J. E.; Kane, A. B.; Black, J. L. *Phys. Rev. Lett.* **1978**, *41*, 1487−1491.
(28) Phillips, W. A. *Rep. Prog. Phys.* **1987**, *50*, 1657−1708.
(29) Fefferman, A. D.; Pohl, R. O.; Zehnder, A. T.; Parpia, J. M. *Phys. Rev. Lett.* **2008**, *100*, 195501.
(30) Lee, C.; Wei, X.; Kysar, J. W.; Hone, J. *Science* **2008**, *321*, 385−388.
(31) Barmatz, M.; Testardi, L. R.; Di Salvo, F. J. *Phys. Rev. B: Condens. Matter Mater. Phys.* **1975**, *12*, 4367−4376.
(32) Jiang, H.; Yu, M.-F.; Liu, B.; Huang, Y. *Phys. Rev. Lett.* **2004**, *93*, 185501.
(33) Hüttel, A. K.; Steele, G. A.; Witkamp, B.; Poot, M.; Kouwenhoven, L. P.; van der Zant, H. S. J. *Nano Lett.* **2009**, *9*, 2547−2552.
(34) Imboden, M.; Mohanty, P. *Phys. Rep.* **2014**, *534*, 89−146.
(35) Anderson, P. W.; Halperin, B. I.; Varma, C. M. *Philos. Mag.* **1972**, *25*, 1−9.
(36) Phillips, W. A. *J. Low Temp. Phys.* **1972**, *7*, 351−360.
(37) Jäckle, J. *Z. Phys. A: Hadrons Nucl.* **1972**, *257*, 212−223.
(38) Kleiman, R. N.; Agnolet, G.; Bishop, D. J. *Phys. Rev. Lett.* **1987**, *59*, 2079−2082.
(39) Venkatesan, A.; Lulla, K. J.; Patton, M. J.; Armour, A. D.; Mellor, C. J.; Owers-Bradley, J. R. *Phys. Rev. B: Condens. Matter Mater. Phys.* **2010**, *81*, 073410.
(40) Rivière, R.; Deléglise, S.; Weis, S.; Gavartin, E.; Arcizet, O.; Schliesser, A.; Kippenberg, T. J. *Phys. Rev. A: At., Mol., Opt. Phys.* **2011**, *83*, 063835.
(41) Esquinazi, P. *Tunneling systems in amorphous and crystalline solids*; Springer Science & Business Media: Berlin, 2013; p 187.
(42) Lulla, K. J.; Defoort, M.; Blanc, C.; Bourgeois, O.; Collin, E. *Phys. Rev. Lett.* **2013**, *110*, 177206.
(43) Faust, T.; Rieger, J.; Seitner, M. J.; Kotthaus, J. P.; Weig, E. M. *Phys. Rev. B: Condens. Matter Mater. Phys.* **2014**, *89*, 100102.
(44) Coppersmith, S. N.; Golding, B. *Phys. Rev. B: Condens. Matter Mater. Phys.* **1993**, *47*, 4922−4936.
(45) Singh, V.; Shevchuk, O.; Blanter, Y. M.; Steele, G. A. *Phys. Rev. B: Condens. Matter Mater. Phys.* **2016**, *93*, 245407.
(46) Remus, L. G.; Blencowe, M. P.; Tanaka, Y. *Phys. Rev. B: Condens. Matter Mater. Phys.* **2009**, *80*, 174103.
(47) Forschungszentrum Jülich GmbH. HNF - Helmholtz Nano Facility, *Journal of large-scale research facilities* **2017**, *3*, A112.

DOI: 10.1021/acs.nanolett.7b01845
Nano Lett. 2017, 17, 5950−5955